Analytical and Experimental Procedures for Determining Propagation Characteristics of Millimeter-Wave Gallium Arsenide Microstrip Lines

Robert R. Romanofsky
Lewis Research Center
Cleveland, Ohio

Summary

In this report, a thorough analytical procedure is developed for evaluating the frequency-dependent loss characteristics and effective permittivity of microstrip lines. The technique is based on the measured reflection coefficient of microstrip resonator pairs. Experimental data, including quality factor Q and effective relative permittivity for 50-Ω lines on gallium arsenide (GaAs) from 26.5 to 40.0 GHz, are presented. The effects of an imperfect open circuit, coupling losses, and loading of the resonant frequency are considered. A cosine-tapered ridge-guide test fixture is described. It was found to be well suited to the device characterization.

Introduction

Fundamentals, Rationale, and Approach

A microstrip line is a geometrically simple transmission line that has found widespread application in microwave circuitry. The structure, illustrated in figure 1, consists of a relatively narrow conducting strip separated from a ground plane by a dielectric material. Because the line can be defined with conventional photolithography techniques, fabrication is quick and inexpensive. The dominant mode of propagation is quasi-TEM (transverse electromagnetic). Because of the two-wire configuration, it has no lower cutoff frequency. Upper frequency limitations are imposed, however, because higher order modes can propagate under certain conditions. Surface waves can be excited when the substrate thickness h approaches half a guide wavelength. In addition, transverse resonance modes can couple to the dominant mode when the guide cross section approaches wavelength dimensions. These constraints limit the maximum usable substrate thickness for a given characteristic impedance.

Numerous theoretical formulations have been proposed to describe the microwave performance of microstrip transmission lines. Accurate analysis is hindered by the inhomogeneous geometry of microstrip, which causes a field discontinuity at the air-dielectric interface. Shortcuts to a full-wave analysis are often employed, particularly when closed-form solutions are desirable. A pure TEM, or static, analysis involves finding a solution for Laplace's equation and the appropriate boundary conditions. This technique ignores any longitudinal field components and neglects transverse currents. A full-wave, or

dynamic, analysis requires solving the Helmholtz equation and is mathematically rigorous. There is a dearth of design information beyond 30 GHz, primarily because the analytical approximations are limited and metrological techniques are inadequate or unavailable. An understanding of the attenuation and phase characteristics is fundamental to providing good models for the behavior at high frequencies. The advent of gallium arsenide (GaAs) monolithic microwave integrated circuit (MMIC) technology has necessitated further investigation in this area. The proliferation of GaAs MMIC's in military systems and their potential application to space communications systems encourage this development. In addition to being the primary interconnect medium, microstrip lines are important in filters and matching circuits. Also, information on attenuation (especially radiation) and dispersion (variation of phase velocity with frequency) is important in patch antenna design.

Many of the procedures to be described in the section "Analytical Evaluation of Microstrip Q" are based on principles outlined by Ginzton (ref. 1) that have been adapted to microstrip "cavities" and modern measurement techniques. Additional work by Aitken (ref. 2) developed alternative methods for evaluating Q from swept-frequency network analysis. The derivations evolved from cavity-equivalent circuits at "detuned open" and "detuned short" measurement planes. This report proceeds through straightforward calculations of the necessary parameters by using a relatively simple but effective model and an innovative measurement technique. A section on the fundamental definition and derivation of Q is included in order to clarify the link between low-frequency descriptions of resonance and the analogy to millimeter-wave cavities. Throughout the report, the terms "cavity" and "resonator" are used interchangeably in referring to microstrip resonant circuits. The usual assumption regarding small losses is adopted in the derivations, that is, $G \gg wC$ and $1/wL$, where G, C, and L are the distributed conductance, capacitance, and inductance per unit length along the transmission line. Note that G should not be interpreted as the shunt conductance due to an imperfect dielectric, which is usually extremely small for microwave substrates. These small losses are normally incorporated as an attenuating exponential modifying the ideal voltage and current distribution. Analogous to the coupling loop that is used to feed a waveguide cavity, a narrow, symmetrical series gap is used to couple to the microstrip resonator. Swept-frequency measurements are performed on an automatic network analyzer
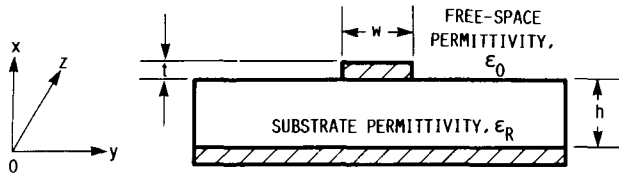
Figure 1.—Microstrip transmission line with propagation in z direction.

by using a cosine-tapered ridge-guide test fixture. The technique is used to determine loss (in terms of Q), dispersion, and fringing effects at the microstrip open circuit.

Losses in Microstrip Lines

Microstrip losses must be accurately quantified in order to predict the performance of microwave circuits. The dominant loss mechanisms for nonmagnetic substrates result from nonideal conductors and dielectrics as well as from radiation. Ohmic losses caused by the finite conductivity of the strip and ground plane account for the greater part of the loss well into the microwave spectrum. The supporting dielectric material, such as GaAs, is usually of very high quality and possesses a small loss tangent. Typical values lie in the range of 0.0001 to 0.001, yielding loss contributions an order of magnitude or more less severe than ohmic and radiation loss. Hence, dielectric loss tends to play a minor role, even at millimeter-wave frequencies. Radiation loss, however, becomes more prevalent with increased frequency. In fact, losses due to radiation can surpass conductor losses at millimeter-wave frequencies to such an extent that shielding techniques are often required.

Skin effect is an important factor with regard to conductor loss. The skin depth is the penetration level into the conductor where the current density has decreased to $1/e$ of its maximum value. As is well known from electromagnetic theory, most of the propagating energy will be contained within a few skin depths of the conductor surface. In fact, if the current distribution were uniquely known, one could calculate the associated attenuation by integrating the current density around the strip and ground plane and invoking the common expression for power transfer and power loss such that

$$\alpha_c = \frac{R_s}{2Z_0} \left[\int_{-w/2}^{w/2} \frac{|J_s|^2}{|I|^2} \, dx + \int_{-\infty}^{\infty} \frac{|J_g|^2}{|I|^2} \, dx \right] \tag{1}$$

where R_s is the surface resistance and J_s and J_g are the current distributions on the center conductor and ground plane, respectively. Hence, the character of the film at the conductor-dielectric interface is largely responsible for determining the attenuation. For example, a thin layer of chromium or titanium is usually deposited on the substrate to promote adhesion of the primary metal. These high-resistivity films can contribute significantly to total loss at higher frequencies. Additionally, the conductivity of the primary metal will be less than the bulk

conductivity because of the deposition process. Porosity and resistivity of the film will depend on the metalization technique. Furthermore, high-temperature sputtering or evaporation can cause diffusion of the adhesion layer into the primary metal. A final point to consider is the surface roughness at the interface, which effectively increases the electrical path length of the signal and results in added loss.

A qualitative description of radiation loss is somewhat more elusive. The effects are prevalent at discontinuities and transitions but defy straightforward analysis. In the case of microstrip resonators, radiation from the abrupt open-circuit line complicates the interpretation of actual line losses. Incidentally, it is interesting to note that a microstrip line behaves as a resonant antenna at integral multiples of one-half wavelength. It must be recognized, however, that the entire microstrip line is radiating, even though the field phase center is located at the apparent aperture occurring from the discontinuity. These effects cause parasitic coupling in microwave circuitry and compromise isolation. Supplemental information on radiation as related to microstrip resonators is provided in the section "Analytical Evaluation of Microstrip Q," particularly in the subsection "Correction for an Imperfect Open Circuit."

Dispersion in Microstrip Lines

Fundamentally, dispersion of an electromagnetic wave is a phenomenon that results when each sinusoidal component shifts in phase as the wavefront travels down a transmission line; therefore, a signal of a particular frequency travels at a specific phase velocity. Phase velocity is the velocity required to maintain an instantaneous phase constant for a given sinusoid. Because microstrip is composed of a mixed dielectric system, a pure TEM mode cannot be sustained. The field components will be contained in both the air and the supporting dielectric material; hence, the relationship between wavelength and velocity becomes complex. As a consequence, the "effective" permittivity will vary at some point between the dielectric constant of the substrate and a static, or zero frequency, value. The effect can be macroscopically interpreted as a hybrid mode resulting from a combination of waves traveling with different phase velocities in the two mediums. This is the source of the quasi-TEM nature of propagation.

Theoretical and experimentally observable constraints describing the behavior of dispersion in microstrip include

(1) A limiting value of permittivity equal to the dielectric constant of the substrate as the frequency tends toward infinity

(2) A minimum effective permittivity near the algebraic mean of the substrate dielectric constant and unity

(3) An effective permittivity that monotonically increases as a function of frequency

Methods for quantifying this behavior range from adapting suitable waveguide models to full-wave spectral domain

analyses, as well as purely empirical techniques. All of these methods suggest that dispersion is strongly dependent on substrate thickness and the relative dielectric constant. Knowledge of this functional dependence is essential for accurate circuit designs. For example, to design a line with a predetermined characteristic impedance, the effective permittivity at the design frequency must be known. Failure to provide high-tolerance impedance matching results in poor return loss and unnecessary performance degradation. The experimental procedures detailed in the section "Permittivity Calculations" provide an accurate technique for evaluating the dispersion phenomenon.

Experimental Procedure

Resonator Techniques

As a consequence of the considerable discrepancies that have appeared in the literature regarding microstrip loss and dispersion, reliable experimental data to complement the theories are necessary. Unfortunately, measurement techniques beyond 30 GHz are not well established. Metrology instrumentation and interface methods tend to be cumbersome and unreliable, particularly for investigating diminutive GaAs devices.

A popular technique at lower frequencies involves the use of microstrip resonators and swept-frequency analysis (refs. 3 and 4). This method involves measuring the reflection coefficient of gap-coupled microstrip resonators. From these data, both the frequency-dependent permittivity $\epsilon_{eff}(f)$ and the unloaded quality factor can be obtained. The techniques developed in later sections of this report enhance the accuracy of the basic procedures.

Linear open-circuit $n\lambda/2$ microstrip resonators were fabricated on 2-in. semi-insulating GaAs wafers along the (100) crystallographic plane in the [0$\bar{1}$0] direction. Both evaporated and electroplated gold films were evaluated to determine the effects of metalization on conductor loss. The technique for determining effective permittivity utilizes two 50-Ω lines on a single die, namely, a short line of length L_1 with a fundamental $\lambda/2$ resonance at F_1, and a long line of length $L_2 \approx 2L_1$ with a first harmonic resonance at $F_2 \approx F_1$. Each line was separated from an adjacent line by a 0.100-in. spacing to avoid coupling effects. By using two lines, the end, or fringing, effects can be excluded from the results (as described in the section "Permittivity Calculations"). The resonators were coupled to the feed line via a critical symmetric gap. The gap dimension was extrapolated from earlier results (refs. 4 and 5). Gap dimensions ranged from 0.00075 to 0.001 in. for 0.005-in.-thick wafers and from 0.0015 to 0.00175 in. for 0.010-in.-thick wafers. Physical line lengths, which are required in the calculation, were resolved to within 2.5 μm with an optical comparator.

Losses were evaluated in terms of the quality factor Q. The unloaded quality factor Q_0 must be derived from the raw data that include the loading effects of the coupling mechanism. Procedures to account for these effects are detailed in the section "Analytical Evaluation of Microstrip Q."

Fabrication of GaAs Microstrip Lines

Two processing techniques were employed to fabricate the microstrip resonators. The first will be identified as "lift-off," for reasons that will become apparent later. The second will be referred to as "pattern electroplating." The processes are illustrated in figure 2. The initial steps of each process are necessarily identical. Prior to the photolithography, the substrates must be thoroughly cleaned. This involves a sequence of solvent and acid soaks to remove contaminants from the wafer surface. After this procedure, the techniques diverge.

In the lift-off process, a layer of positive photoresist is spin coated at high rotational speed to obtain a uniform film. Positive photoresist is a photosensitive polymer that becomes soluble in developing solvents after being exposed to ultraviolet (UV) light. Next, the wafer is exposed to the UV light through a negative or dark-field chromium-glass mask. At this point, the desired pattern has been transferred to the wafer. The coated wafer is then soaked in chlorobenzene, which slightly penetrates the resist layer. This step makes the top surface of the resist impervious to development, causing an overhang structure to be formed during patterning. Following development, a 200-Å layer of titanium is evaporated onto the entire surface to enhance adhesion. Subsequently, the primary metal layer of gold is deposited. The final step in the photolithography process involves the lift-off action. The resist is removed in acetone or a similar solvent. The overhang structure that was formed earlier makes possible the penetration of the solvent beneath the metalization that had been evaporated over the entire surface.

In pattern electroplating, a 200-Å titanium layer is deposited, followed immediately by a 1000-Å gold deposition. This occurs prior to any photolithography. Next, a layer of positive photoresist is spin coated onto the wafer and then exposed through the same dark-field mask. The wafer is then developed, and windows, corresponding to the desired circuit pattern, are established. This process permits the selective deposition of metal because only the exposed sections of the wafer will be plated. The actual electroplating entails submersing the wafer in an aqueous gold-potassium-cyanide solution. A platinum-titanium anode is connected to a constant-current source and the wafer, which becomes the cathode, is grounded. The process is extremely sensitive to a number of variables, including current density, bath temperature, pH, agitation, and ion content. The process is often plagued by photoresist degradation caused by long plating times as well as by hydrogen co-deposition, which deteriorates the gold deposit. It is desirable to minimize the plating time because
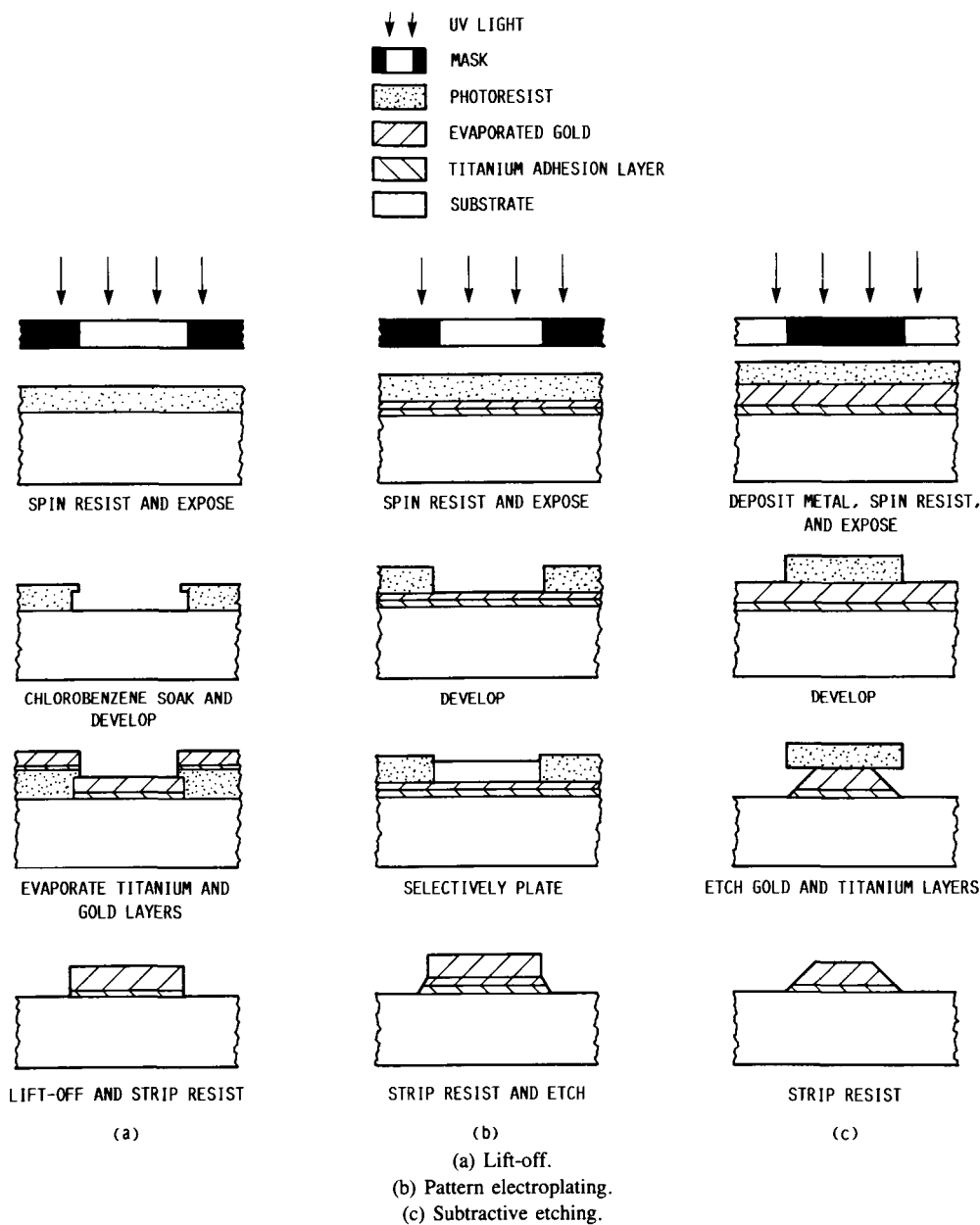
Figure 2.—Comparison of photolithographic circuit fabrication techniques.

Legend:
- UV LIGHT
- MASK
- PHOTORESIST
- EVAPORATED GOLD
- TITANIUM ADHESION LAYER
- SUBSTRATE

Column (a):
SPIN RESIST AND EXPOSE
CHLOROBENZENE SOAK AND DEVELOP
EVAPORATE TITANIUM AND GOLD LAYERS
LIFT-OFF AND STRIP RESIST
(a)

Column (b):
SPIN RESIST AND EXPOSE
DEVELOP
SELECTIVELY PLATE
STRIP RESIST AND ETCH
(b)

Column (c):
DEPOSIT METAL, SPIN RESIST, AND EXPOSE
DEVELOP
ETCH GOLD AND TITANIUM LAYERS
STRIP RESIST
(c)

(a) Lift-off.
(b) Pattern electroplating.
(c) Subtractive etching.

of interaction between the photoresist and the electrolyte. Additionally, the resistance of the bath can change dramatically during the process, making it difficult to regulate the current and thus the thickness and quality of the film. A variable/constant current source was designed to alleviate a number of fabrication problems (fig. 3). This source will provide the desired constant current over a wide range of load conditions. Specifically, the supply will deliver up to 500 mA for a load ranging from essentially zero to 200 Ω and 10 mA for a load up to 10 000 Ω. The current density required to deposit high-quality films on GaAs is approximately 3 mA/in.^{2} A set of curves giving deposition rates for various circuit areas is provided in figure 4. These graphs tend to overestimate the film thickness somewhat because they assume 100 percent current efficiency. The final step in this process is the removal of the thin underlying layer of gold and titanium. This layer can be removed by using chemical (acid etch) techniques or mechanical ion milling. Although a thin layer of the primary gold will also be removed, the effect is insignificant because the films are usually plated to at least 2 μm. Table I summarizes the post-photolithography electroplating process.

Both techniques are attractive because each one results in well-defined geometries with little undercutting. The additive process overcomes the drawbacks associated with a subtractive
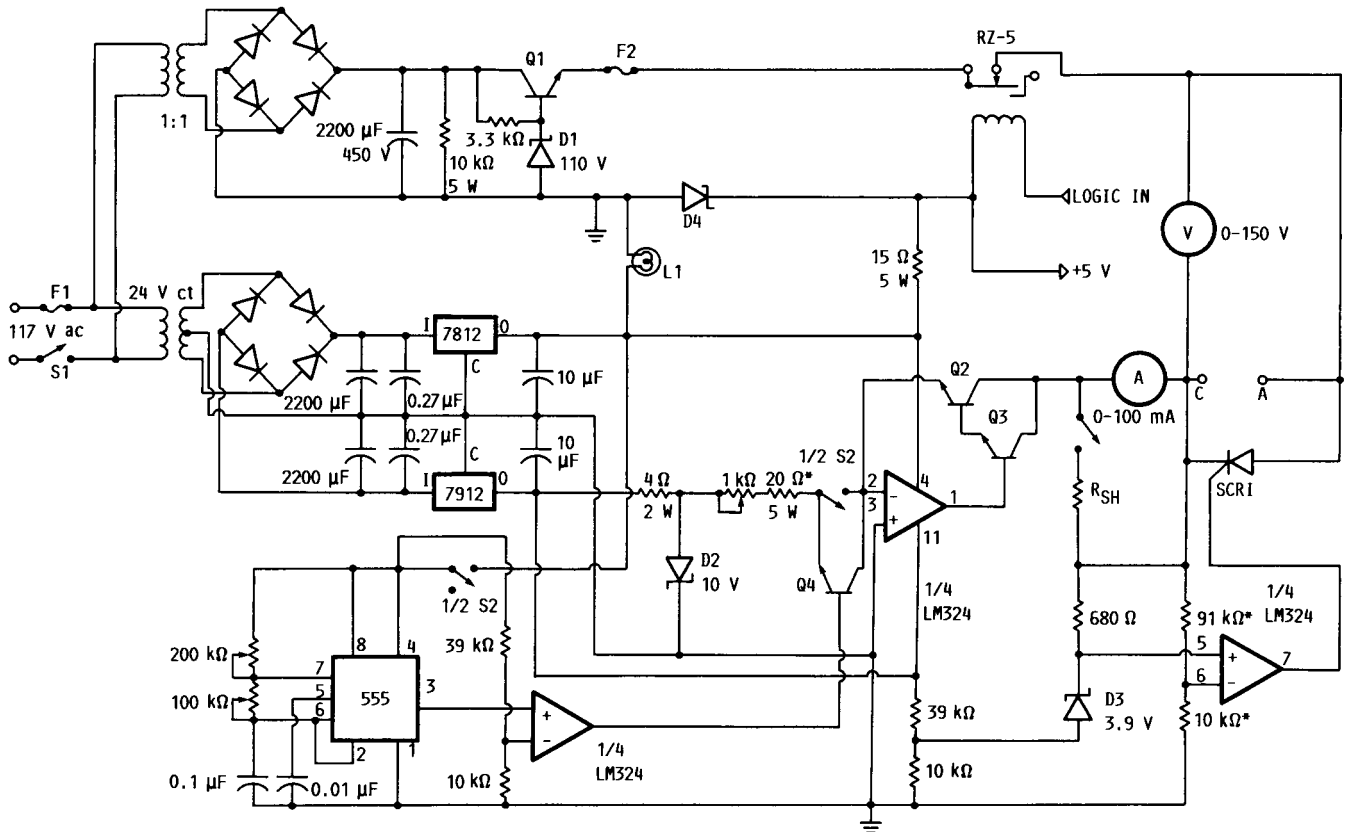
Figure 3.—Schematic of analog portion of variable/constant current source used for plating.

etching process. Depending on the density and topography of the wafer to be processed, pattern plating can be desirable because it conserves precious metals.

The wafers must be lapped and polished to a specific thickness in order to obtain the correct characteristic impedance. This is a critical step because of the fragile nature of the substrates. Lapping is primarily a mechanical process that uses a silicon carbide or alumina slurry and a slowly rotating platen to remove GaAs. This process produces a very rough surface. In order to obtain a device-quality surface, the GaAs must be polished to optical flatness. This is accomplished by using a combination of chemical and mechanical action. An aqueous solution of Clorox (sodium hypochlorite) and colloidal silica is dispensed on an almost identical platen covered with a feltlike pad rotated at a much higher speed. This process yields a mirror finish onto which a titanium-gold ground plane is evaporated.

Device Characterization

In order to obtain the reflection coefficient of the microstrip resonators, S-parameter measurements were performed on an automatic network analyzer (ANA). Because the measurements were extremely sensitive to frequency, a synthesized generator was used for the radiofrequency source. The system was calibrated in a WR–28 waveguide (26.5 to 40.0 GHz) by using through-short-load standards supplied by the manufacturer. The most imposing obstacle was the interface between the waveguide and the GaAs microstrip lines. In general, metrological techniques at these frequencies are not well established. Because there are no known commercially available test fixtures above 26.5 GHz, a new fixture had to be developed to test the devices.

In conjunction with an MMIC characterization project at NASA Lewis, a cosine-tapered ridge-guide transition was developed to test high-frequency devices. The transition is an

(a) Surface area, 0 to 0.05 in.^{2}.
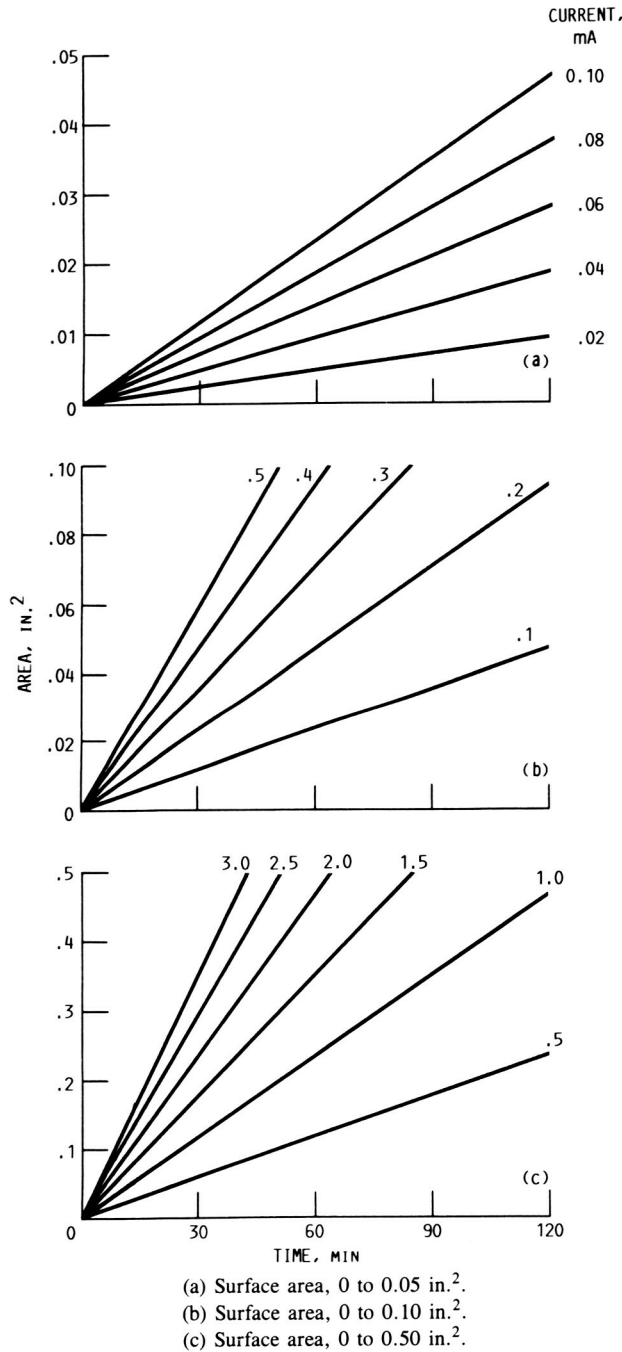(b) Surface area, 0 to 0.10 in.^{2}.
(c) Surface area, 0 to 0.50 in.^{2}.

Figure 4.—Deposition rates for 2.5-μm-thick gold film.

TABLE I.—POST-PHOTOLITHOGRAPHY ELECTROPLATING
PROCESS GP-1.

[Plating base: 200 Å titanium; 1000 Å gold; 100 Å titanium (optional).]

Step	Description
1.	Use a wafer with ≈ 2 μm of photoresist protection on the back
[a]2.	50 Percent HCl (hydrochloric acid) for 30 sec
[a]3.	De-ionized water rinse
[a]4.	5 Percent HF (hydrofluoric acid) until thin titanium layer is removed (≈ 15 sec)
[a]5.	De-ionized water rinse
6.	50 Percent HCl for 30 sec
7.	De-ionized water rinse
8.	Gold plate ≈ 2 μm at 0.5 A/ft^2 and 140 °F
9.	Remove photoresist (acetone-alcohol-rinse)
[a]10.	5 Percent HF until thin titanium layer is removed (≈ 15 sec)
[a]11.	De-ionized water rinse
12.	KI (potassium iodide) etch until thin gold layer is removed (≈ 5 sec)
13.	De-ionized water rinse
14.	5 Percent HF until titanium layer is removed (≈ 25 sec)
15.	De-ionized water rinse
16.	Dry (N$_2$)

[a]Skip this step if second layer of titanium is not used.

"Analytical Evaluation of Microstrip Q" deals with this problem. The fixture used in these experiments is illustrated in figure 5.

The resonator chips were mounted beneath the ridge by pressure contact. In order to obtain all the required information, a listing of the S_{11} data, as well as the corresponding Smith chart for each resonator, was obtained. Information in subsequent sections describes the data reduction techniques.
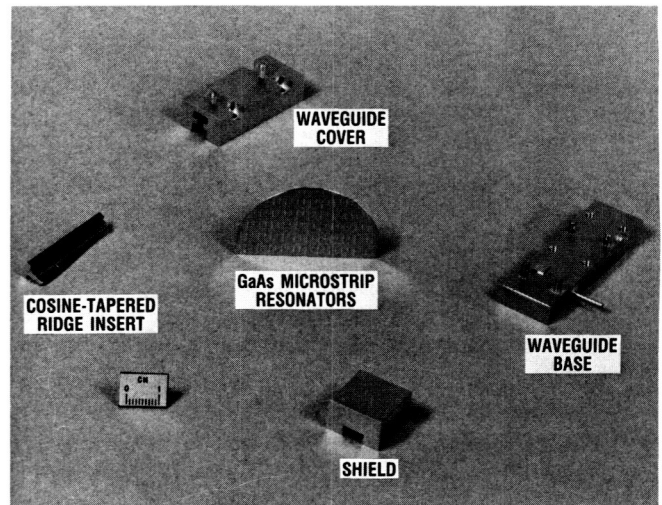

Figure 5.—Test fixture.

E-plane taper that serves as a transformer between the high-impedance waveguide and the 50-Ω microstrip. A detailed account of a fixture utilizing this technique is provided in reference 6. This fixture has the capability of positioning the reference, or measurement, plane at a more desirable location. Judicious positioning of the reference plane can prevent complications from the resonator feed line. The section

Analytical Evaluation of Microstrip Q

Definition of Q and Relationship to Bandwidth

The quality factor of a cavity, which is a measure of frequency selectivity, is formally defined as

$$Q \equiv \text{Internal } Q \text{ of cavity} \equiv \frac{2\pi(\text{Energy stored})}{\text{Energy loss/cycle}} = \frac{2\pi W}{P}$$

(2)

An isolated microwave cavity in the vicinity of resonance can be accurately represented by an RLC tank circuit. This lumped-element, equivalent circuit concept neglects the effects of additional poles in the impedance function that result from higher order modes (ref. 7). In particular, an open-circuit microstrip line will resonate at a fundamental frequency ω_0 and an infinite number of harmonics. Typically, the resonances are far enough apart so as not to perturb the equivalent circuit of the moderate-to-high Q cavity. Proceeding with the lumped-element model, Q_0 can be derived as follows. The driving point admittance is

$$Y = \frac{1}{R} + j\left(\omega C - \frac{1}{\omega L}\right)$$

(3)

The susceptance vanishes at the resonant frequency $\omega = \omega_0$. Therefore, ω_0 must equal $1/\sqrt{LC}$, where L and C are the distributed inductance and capacitance of the transmission line. It is important to realize that these parameters must be uniquely determined for a specific mode.

Let the voltage across R_0 at resonance be described by

$$v(t) = R_0 I_m \cos \omega_0 t$$

(4)

where R_0 represents ohmic, dielectric, and radiation losses associated with the cavity and I_m is the maximum current. Then the energy stored in the electric field becomes

$$W_c(t) = \frac{C_0 R_0^2 I_m^2 \cos^2 \omega_0 t}{2}$$

(5)

and the energy stored in the magnetic field is

$$W_L(t) = \frac{L\left(\dfrac{1}{L}\displaystyle\int_0^t R_0 I_m \cos \omega_0 t \, dt\right)^2}{2}$$

(6)

Thus, the total instantaneous energy in the electric and magnetic fields is equal to

$$W(t) = W_c(t) + W_L(t) = \frac{I_m^2 R_0^2 C_0}{2}$$

(7)

The total energy loss per period is equal to the average power delivered to the circuit multiplied by $2\pi/\omega_0$. Hence,

$$P = \frac{2\pi}{\omega_0}\frac{1}{T_0}\int_0^{T_0} R_0 I_m^2 \cos^2 \omega_0 t \, dt = \frac{I_m^2 R_0}{2 f_0}$$

(8)

and

$$Q_0 = 2\pi f_0 R_0 C_0 = R_0 C_0 \omega_0$$

(9)

Input admittance can be expressed in terms of the unloaded quality factor as follows:

$$Y(j\omega) = \frac{1}{R} + j\frac{1}{R}\left(\omega C R - \frac{R}{\omega L}\right)$$

(10)

$$Y(j\omega) = \frac{1}{R}\left[1 + j\left(\frac{\omega Q_0}{\omega_0} - \frac{Q_0/\omega_0 C}{\omega L}\right)\right]$$

(11)

$$Y(j\omega) = \frac{1}{R}\left[1 + jQ_0\left(\frac{\omega}{\omega_0} - \frac{\omega_0}{\omega}\right)\right]$$

(12)

From this point forward, it will be more convenient to describe the reciprocal of Y because the measured results will correspond to impedance data.

$$Z(j\omega) = \frac{R}{1 + jQ_0\left(\dfrac{\omega}{\omega_0} - \dfrac{\omega_0}{\omega}\right)}$$

(13)

By invoking the low-loss assumption, it is clear that R must be very large because the impedance tends toward infinity for a parallel resonant circuit. For mathematical simplicity, the

half-power, or 3-dB, bandwidth is usually considered. This implies that

$$Q\left(\frac{\omega_1}{\omega_0} - \frac{\omega_0}{\omega_1}\right) = -1 \tag{14}$$

and

$$Q\left(\frac{\omega_2}{\omega_0} - \frac{\omega_0}{\omega_2}\right) = 1 \tag{15}$$

In solving for the 3-dB frequencies, one obtains

$$\omega_1 = \omega_0 \left\{ \left[1 + \left(\frac{1}{2Q_0}\right)^2\right]^{1/2} - \frac{1}{2Q_0} \right\} \tag{16}$$

and

$$\omega_2 = \omega_0 \left\{ \left[1 + \left(\frac{1}{2Q_0}\right)^2\right]^{1/2} + \frac{1}{2Q_0} \right\} \tag{17}$$

In solving for the 3-dB bandwidth, one obtains

$$\omega_2 - \omega_1 = \frac{\omega_0}{Q_0} \tag{18}$$

Alternatively, the familiar expression for the quality factor becomes

$$Q_0 = \frac{\omega_0}{\omega_2 - \omega_1} = \frac{f_0}{f_2 - f_1} \tag{19}$$

Notice that the phase of $Z(j\omega)$ is $\pm 45°$ at the half-power bandwidth and $0°$ at resonance. Although it is possible to evaluate the Q with phase information exclusively, the amplitude measurement accuracy is superior. In addition, coupling loss can be determined readily from the magnitude data. The technique to be described requires both phase and magnitude information for an unambiguous determination of Q_0. This technique is not recommended for highly overcoupled cavities, for which the impedance locus circle expands toward the periphery of the Smith chart.

Definition and Derivation of Coupling Coefficient

The resonant circuit just described can be completely defined by specifying ω_0, Q_0, and R_0 for a given mode. Because the microwave cavity must be coupled to a transmission line for the measurements to be performed, the input impedance will be modified. The following derivation assumes that the R, L, and C values are frequency independent near resonance and therefore frequency independent over the entire measurement range. In general, the coupling between the resonator and the transmission feed line contains resistive and reactive elements. This coupling loss component and the characteristic impedance of the transmission line load the resonant circuit. Thus, the measured Q, denoted by Q_L, will differ from the desired Q described earlier, and Q_0 now is defined as the unloaded quality factor representing the characteristics of the resonator if it were not perturbed by the coupling mechanism. In a microstrip resonator, the coupling is accomplished by using a narrow ($\ll \lambda g$) gap. This discontinuity can be modeled by a capacitive π network, or equivalently, by an ideal transformer, as illustrated in figure 6.

The effect of loading is to increase the conductance of the resonator by an amount equal to the transmission-line characteristic admittance multiplied by the transformer turns ratio n. Hence, the modified Q will be smaller and is given by

$$Q_L = \frac{\omega C_0}{G_0 + n^2 Y_0} \tag{20}$$

It is assumed that the coupled susceptance is negligible compared with the resonator susceptance. A comparison of Q_L with Q_0 yields

$$\frac{1}{Q_L} = \frac{1}{Q_0} + \frac{n^2 Y_0 / G_0}{Q_0} \tag{21}$$

where $n^2 Y_0 / G_0$ is the ratio of coupled conductance to resonator conductance and is referred to as the coupling coefficent κ. Because G_0 is very small, n must be less than 1 for reasonable values of κ.

The unloaded quality factor may therefore be expressed as
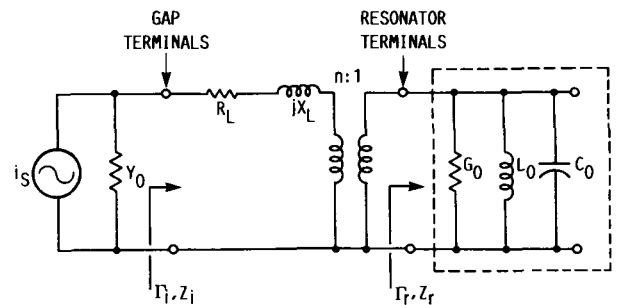
$$Q_0 = (1 + \kappa)Q_L \tag{22}$$

Figure 6.—Lumped-element equivalent circuit representation of open microstrip resonator coupled to matched source near resonance.

On the basis of the preceding equivalent circuit, the input impedance is

$$Z_i(j\omega) = R_L + jX_L + \frac{\kappa Z_0}{1 + jQ_0\left(\dfrac{\omega}{\omega_0} - \dfrac{\omega_0}{\omega}\right)} \qquad (23)$$

It is apparent that the coupling gap will function as an impedance inverter and result in a small reflection coefficient at resonance. Reactance jX_L is associated with the coupling system and is caused by fringing fields at the gap discontinuity. (It is also possible to embody the effects of higher order modes in this equivalent reactance (ref. 8).) The coupling reactance tends to shift the resonant frequency slightly and can be ignored during the loss measurements. Because ΔF is small and the attenuation does not vary appreciably over the narrow range, the effect on Q_0 is insignificant. The coupling loss R_L is also temporarily ignored. From equation (23), the reflection coefficient at the input of the coupling network is

$$\Gamma_i = \frac{\kappa Z_0 - Z_0(1 + j2Q_0\delta)}{\kappa Z_0 + Z_0(1 + j2Q_0\delta)} \qquad (24)$$

with the substitution $(\omega^2 - \omega_0^2)/\omega\omega_0 \approx 2\delta = 2\left(\dfrac{\omega - \omega_0}{\omega_0}\right)$, which is valid for moderate- and high-Q cavities.

In terms of Q_L, the reflection coefficient becomes

$$\Gamma_i = \frac{(\kappa - 1)/(\kappa + 1) - j2Q_L\delta}{1 + j2Q_L\delta} \qquad (25)$$

At resonance, the reactive terms disappear and

$$\Gamma_{io} = \frac{\kappa - 1}{\kappa + 1} \qquad (26)$$

Note that in this equation, the magnitude of Γ_{io} remains unchanged if κ is replaced with its reciprocal. Critical coupling occurs when the resonator is matched to the source and consequently $\kappa = 1$. When $\kappa < 1$, the resonator is undercoupled and is defined by

$$\kappa = \frac{1 - |\Gamma_{io}|}{1 + |\Gamma_{io}|} \equiv \mathrm{VSWR}^{-1} \qquad (27)$$

Conversely, when the resonator is overcoupled, $\kappa > 1$ and is defined by

$$\kappa = \frac{1 + |\Gamma_{io}|}{1 - |\Gamma_{io}|} \equiv \mathrm{VSWR} \qquad (28)$$

To determine if the resonator is overcoupled or undercoupled, one can consider the impedance locus on a Smith chart. The expression for Γ can be rewritten as

$$\Gamma_i = \frac{\kappa - (1 + j2Q_0\delta)}{\kappa + (1 + j2Q_0\delta)} + \frac{\kappa + (1 + j2Q_0\delta)}{\kappa + (1 + j2Q_0\delta)} - 1 \qquad (29)$$

Hence,

$$\Gamma_i + 1 = \frac{2\kappa}{\kappa + 1 + j2Q_0\delta} \qquad (30)$$

The vector $\Gamma_i + 1$ traces a circle on the Smith chart with a diameter d of $2\kappa/(\kappa + 1)$. This is illustrated in figure 7 for an undercoupled resonator.

The degree of coupling can therefore be determined from an inspection of the Smith chart impedance plot. The three possibilities correspond to $d = 1$ (critically coupled), $d < 1$ (undercoupled), and $d > 1$ (overcoupled). Note that the angle ϕ of the $\Gamma + 1$ vector is given by

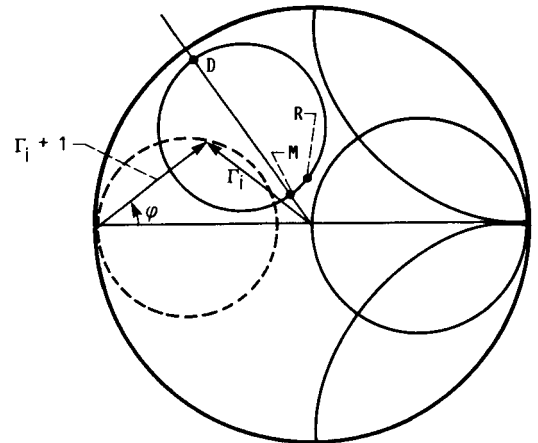$$\phi = \tan^{-1}\left(\frac{2Q_0\delta}{\kappa + 1}\right) \qquad (31)$$

Figure 7.—Ideal impedance locus for undercoupled resonator (dashed line) and translated locus in presence of coupling loss and reactance. Point D, detuned resonator; point R, unloaded resonant frequency; point M, loaded resonant frequency; Γ_i, input reflection coefficient.

An actual measured locus would be shifted by $R + jX$, where R and X represent the coupling resistance and reactance, respectively. The minimum reflection coefficient occurs at point M, which designates the resonant frequency of the loaded resonator. Point D corresponds to the complex impedance of the coupling circuit and represents a completely detuned resonator. Point R represents the unloaded resonant frequency. A procedure to account for the loading effect is developed in a later section.

Measurement of Unloaded Quality Factor Q_L

The reflection coefficient amplitude response curve of an overcoupled resonator is very broad. Correspondingly, for a given Q_0, the loaded Q will be relatively small. An undercoupled resonator will exhibit a sharp response, but the reflection coefficent magnitude will be small. Figure 8 exhibits this behavior. In either case, the effect of coupling must be considered when measuring the loaded Q. The reflection coefficient at the half-power bandwidth is obtained by setting $|j2Q_0\delta| = 1$. At these frequencies, the input impedance of the resonator has diminished by a factor of $1/\sqrt{2}$ and the power coupled to the cavity is one-half the power coupled at resonance. Hence, Q_L is determined when the reflection coefficient attains a value given by

$$
\begin{aligned}
\left| \Gamma_{i,1/2} \right| &= \left[\frac{(\kappa - 1)/(\kappa + 1)^2 + 1}{2} \right]^{1/2} \\
&= \left[\frac{\kappa^2 - 2\kappa + 1 + \kappa^2 + 2\kappa + 1}{2(\kappa + 1)^2} \right]^{1/2} \quad (32)
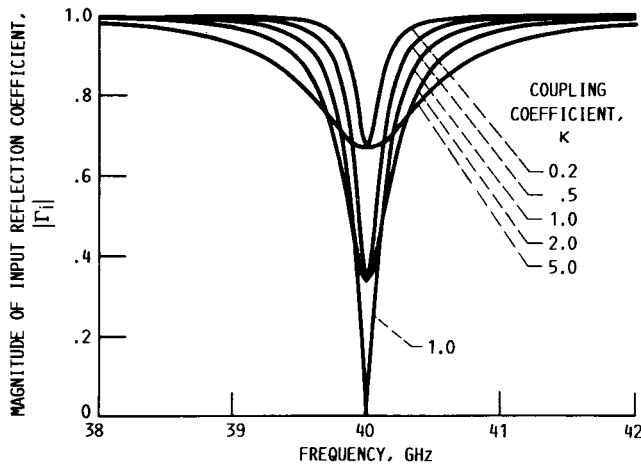\end{aligned}
$$

Figure 8.—Typical resonator reflection coefficient magnitude with various degrees of coupling for $Q_0 = 100$ in absence of series loss.

Therefore, the measured magnitude of the reflection coefficient at the 3-dB bandwidth is

$$
\rho_{1/2} = 10 \log_{10} \left[\frac{\kappa^2 + 1}{(\kappa + 1)^2} \right] dB \quad (33)
$$

and the loaded Q can be calculated from equation (19), where $f_2 - f_1$ is the bandwidth at the level $\rho_{1/2}$. The corresponding voltage standing wave ratio (VSWR) is equal to

$$
\frac{(\kappa + 1) + (\kappa^2 + 1)^{1/2}}{(\kappa + 1) - (\kappa^2 + 1)^{1/2}} \quad (34)
$$

Effects of Small Coupling Loss on Q Factors

A complete description of the input impedance at the terminals of the coupling network was specified by equation (23). The reactance term jX_L is assumed to be frequency independent over the measurement range and does not influence the interpretation of the coupling parameter. However, the coupling loss modifies the location of the half-power points, thus changing Q_L. It also results in a slightly different κ. In the presence of coupling loss, the reflection coefficient far off resonance is

$$
\Gamma_\infty = \frac{(R_L/Z_0) - 1}{(R_L/Z_0) + 1} = \frac{\sigma - 1}{\sigma + 1} \quad (35)
$$

The effect is perceived as a linear displacement on the Smith chart by an amount σ. Consequently, the log of the reflection coefficient no longer tends toward zero away from resonance. Similarly, at resonance, the reflection coefficient logarithm attains some finite value. The impedance locus shifts by σ and the effective κ, denoted κ', becomes

$$
\kappa' = \sigma + \kappa \quad (36)
$$

By including the contribution from coupling loss, the input impedance becomes

$$
Z_i = \kappa' \left[\gamma Z_0 + \frac{Z_0(1 - \gamma)}{1 + j2Q_0\delta} \right], \quad \text{where} \quad \gamma = \frac{\sigma}{\kappa'} \quad (37)
$$

The corresponding reflection coefficient can be derived as follows:

$$
\Gamma_i = \left[\frac{R_L(1 + j2Q_0\delta) + \kappa Z_0 - Z_0(1 + j2Q_0\delta)}{R_L(1 + j2Q_0\delta) + \kappa Z_0 + Z_0(1 + j2Q_0\delta)} \right] \quad (38)
$$

$$\Gamma_i = \left[\frac{\sigma(1 + j2Q_0\delta) + \kappa - (1 + j2Q_0\delta)}{\sigma(1 + j2Q_0\delta) + \kappa + (1 + j2Q_0\delta)} \right] \quad (39)$$

Finally,

$$\Gamma_i = \left[\frac{(\sigma + \kappa - 1) + j2Q_0\delta(\sigma - 1)}{(\sigma + \kappa + 1) + j2Q_0\delta(\sigma + 1)} \right] \quad (40)$$

Figure 9 portrays typical responses of 20 log $|\Gamma_i|$ as a function of frequency for $\omega_0 = 40$ GHz. Notice that 2.5 Ω of series loss ($\sigma = 0.05$) results in almost 1 dB of return loss degradation.

In terms of Q_L, Γ_i becomes

$$\Gamma_i = \frac{(\kappa' - 1) + j2Q_L\delta \left[(\sigma - 1)/(\sigma + 1)\right](\kappa' + 1)}{(\kappa' + 1) + j2Q_L\delta \ (\kappa' + 1)} \quad (41)$$

Upon simplification,

$$\Gamma_i = \frac{(\kappa' - 1)/(\kappa' + 1) + j2Q_L\delta \left[(\sigma - 1)/(\sigma + 1)\right]}{1 + j2Q_L\delta} \quad (42)$$

At the 3-dB bandwidth, $|j2Q_L\delta| = 1$ and

$$\Gamma_{i,1/2} = \frac{(\kappa' - 1)/(\kappa' + 1) + j \left[(\sigma - 1)/(\sigma + 1)\right]}{1 + j} \quad (43)$$
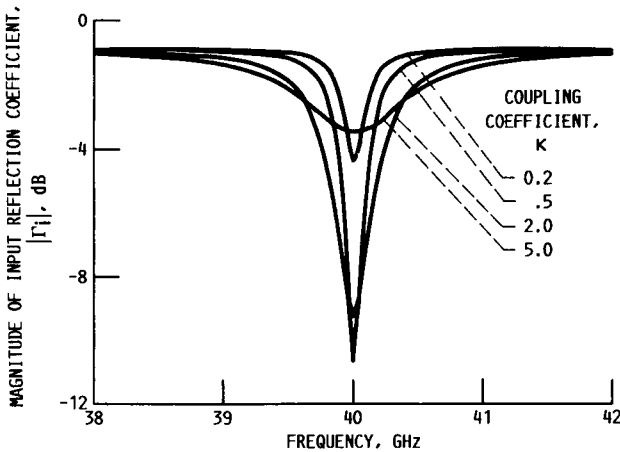

Figure 9.—Typical resonator reflection coefficient (log) magnitude with various degrees of coupling for $Q_0 = 100$ in presence of series loss ($\sigma = 0.05$).

which implies

$$\rho_{1/2} = 10 \log_{10} \frac{\left[(\kappa' - 1)/(\kappa' + 1)\right]^2 + \left[(\sigma - 1)/(\sigma + 1)\right]^2}{2} \text{ dB} \quad (44)$$

This is the level at which the new loaded Q must be determined. Notice that $\rho_{1/2}$ reduces to $\rho_{1/2}$ for lossless coupling as $\sigma \to 0$. The value of σ can be calculated from the magnitude of the reflection coefficient far off resonance according to

$$\sigma = \frac{1 - |\Gamma_\infty|}{1 + |\Gamma_\infty|}, \quad \text{for } R_L < Z_0 \quad (45)$$

On the basis of the equivalent circuit model, with loss element R_L external to the resonator, Q_L can be expressed as

$$Q_L = \frac{\omega_0 C_0}{G_0 + n^2[1/(Z_0 + R_L)]} \quad (46)$$

$$\frac{1}{Q_L} = \frac{1}{Q_0} + \frac{1}{Q_0} \left[\left(\frac{n^2}{G_0}\right)\left(\frac{1}{Z_0 + R_L}\right) \right]$$
$$= \frac{1}{Q_0} \left(1 + \frac{n^2}{G_0 Z_0 + G_0 R_L} \right) \quad (47)$$

$$\frac{1}{Q_L} = \frac{1}{Q_0} \left[\frac{1 + (R_L/Z_0) + (n^2/G_0 Z_0)}{1 + (R_L/Z_0)} \right] = \frac{1}{Q_0} \left(\frac{1 + \sigma + \kappa}{1 + \sigma} \right) \quad (48)$$

Finally, the revised value for Q_0 becomes

$$Q_0 = Q_L \left(\frac{1 + \kappa'}{1 + \sigma} \right) \quad (49)$$

Correction for an Imperfect Open Circuit

The measured Q will include losses associated with radiation from the abrupt open-circuit line as well as some disturbance from the parasitic fringing capacitance. The end effect, which
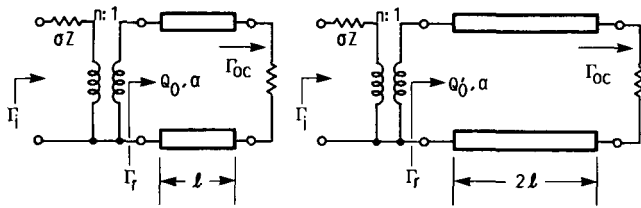
Figure 10.—Equivalent representation for pair of microstrip resonators with fundamental ($\lambda/2$) and first harmonic (λ) resonance, where Γ_{oc} is low-loss open circuit.

causes $|\Gamma_{oc}|$ to be less than unity, can be evaluated by using two resonators as described in the following paragraph. The situation is illustrated in figure 10.

The isolated resonator reflection coefficient is equal to

$$\Gamma_r = e^{-2\alpha\ell} e^{-2\alpha_r} e^{-j2\beta\ell} e^{-j2\theta_r} \qquad (50)$$

where α and β represent the attenuation and phase constants of the cavity for a perfect open circuit. The open-circuit radiation loss is identified as α_r. The open-circuit reactance $e^{-j2\theta_r}$, which causes a small phase shift, will be ignored because its influence on the Q measurement is minor. The reactance is often treated as a hypothetical line extension of approximately 0.3 to 0.5 substrate thickness. If the conventional relationship between Q and α is modified to account for the additional loss, one obtains

$$Q_0 \approx \frac{\pi}{\lambda_{g0}\left(\alpha + \dfrac{\alpha_r}{\ell}\right)} \approx \frac{\pi}{2\ell\left(\alpha + \dfrac{\alpha_r}{\ell}\right)} \qquad (51)$$

and

$$Q_0' \approx \frac{\pi}{\lambda_{g0}'\left(\alpha + \dfrac{\alpha_r}{\ell'}\right)} \approx \frac{\pi}{2\ell\left(\alpha + \dfrac{\alpha_r}{2\ell}\right)} \qquad (52)$$

In these equations, $\lambda_{g0} = 2\ell/n$ and $\lambda_{g0}' = 2\ell'/n$, where n is an integer corresponding to the order of resonance. This is analogous to the expression obtained for a waveguide cavity with a lossy endplate (ref. 9). The difference between the guide wavelengths λ_{g0} and λ_{g0}' is small. More precisely, the fundamental frequency ($n = 1$) of the short resonator is nearly equal to the first harmonic ($n = 2$) of the long resonator. Hence, the open-circuit loss can be assumed to be identical in each instance. The implication, therefore, is that α_r is independent of resonator length over at least one octave. Previous studies have indicated that fringing is primarily a function of substrate and geometry (refs. 10 and 11). It is

important to convey that α_r does not represent the radiation losses of the entire resonator but strictly the open-circuit effect. In solving for α by using equations (51) and (52), one obtains

$$\alpha = \frac{\pi}{2\ell}\left(\frac{2}{Q_0'} - \frac{1}{Q_0}\right) \text{ nepers/unit length} \qquad (53)$$

This definition for Q is not strictly correct because the transmission line is dispersive. As a consequence, the phase velocity v_p differs from the group velocity v_g. In general, the group velocity exceeds the phase velocity for a two-wire transmission line, with the difference diminishing as the frequency increases.

The exact expression for Q, in the absence of end effects, is (ref. 12)

$$Q_0 = \frac{\omega d\beta/d\omega}{2\alpha} \qquad (54)$$

Although some deviation exists, the approximation is valid well into millimeter wavelengths for 50-Ω lines on thin (<0.010 in.) GaAs. This can be demonstrated by calculating the frequency-dependent permittivity and comparing $\epsilon_{eff}(f)/\omega$ with $d\epsilon_{eff}(f)/d\omega$. Low impedance lines or thick substrates (particularly those with a high dielectric constant) may necessitate using the relationship expressed by equation (54).

Interpretation of Impedance Locus

The value X/Z_0 is the normalized self-reactance of the coupling system and is equal to the imaginary portion of the input impedance when the resonator is completely decoupled. If the actual measurement plane is positioned coincident with the reference plane, X/Z_0 can be read directly from the Smith chart impedance plot at point D (fig. 7). In practice, however, the measurement plane is located beyond the transformer terminals, and the resulting reflection coefficient is shifted by approximately $e^{-2j\beta\ell}$. This precludes a direct graphic measurement of the reactance because the impedance locus will be rotated clockwise by an amount $2\beta\ell$. Because β is a function of frequency, additional distortion of the locus occurs as points of higher frequency sweep through a greater translation. The actual trace can appear as a loop if the input feed line is electrically long. A Smith chart plot of this phenomenon is provided in figure 11. The data were generated with a commercially available software package and are based on the model of figure 6. This length should be minimized in order to avoid errors in the Q calculation. De-embedding techniques are available that enable the actual measurement plane to be relocated to the ideal measurement terminals. By means of a through-short-delay calibration algorithm and a cosine-tapered ridge-guide fixture, the measurement plane could be positioned adjacent to the microstrip gap.
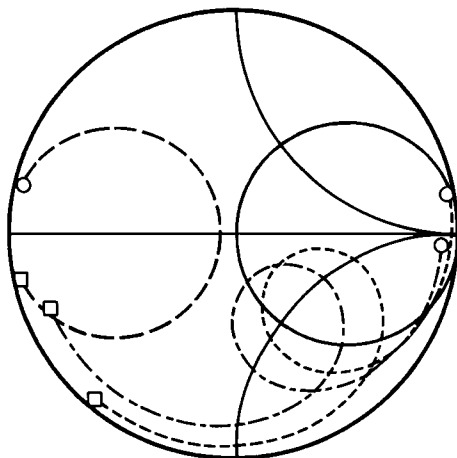
Figure 11.—Modeled effect of feed line on hypothetical resonator.

Permittivity Calculations

Dispersion Measurements

Rigorous descriptions of microstrip dispersion are available; however, quasi-static and semiempirical equations tend to be better suited for implementation. Experimental data to complement the various theories are limited, especially at millimeter wavelengths for semiconductor substrates. The mechanism responsible for the dispersive behavior that causes the phase velocity to decrease with frequency is not well understood. The technique for deriving the effective permittivity from measured parameters has been previously documented and is repeated here for completeness (ref. 4). The experimental arrangement is represented schematically in figure 12.

It is assumed that both the gap and open-end fringing are independent of resonator length with the additional constraint of identical coupling gaps. If the sum of the fringing lengths at the gap and open end is designated as ℓ_e, then

$$\ell_1 + \ell_e = \frac{\lambda_g}{2} \tag{55}$$

and

$$\ell_2 + \ell_e = \lambda_g \tag{56}$$

The assumption that ϵ_{eff} is constant between the fundamental of the short resonator and the first harmonic of the long resonator leads to

$$\epsilon_{eff}(f) = \left[\frac{c(2f_1 - f_2)}{2f_1 f_2(\ell_2 - \ell_1)} \right]^2 \tag{57}$$

where c is the speed of light in vacuum. The total end-effect length can be calculated by dividing equation (55) by equation (56) and solving for ℓ_e.

$$\ell_e = \frac{f_2\ell_2 - 2f_1\ell_1}{2f_1 - f_2} \tag{58}$$

Normally, the coupling between the feed line and the resonator is minimized to suppress frequency pulling. Even slight loading of the resonator will affect the measured frequency. The section "Perturbation of Natural Resonant Frequency Due to Loading" describes a procedure to account for the difference between the apparent and natural resonant frequency of the cavity.

The assumption regarding identical coupling is realistic because of the high degree of reproducibility possible with conventional photolithography and the exceptional control of substrate parameters. However, it is possible and certainly instructive to consider the ratio of reflection coefficients on the resonator side of the coupling gap. The input impedance looking into the isolated resonator in terms of the measured quantities is

$$Z_r = \frac{Z_i - \sigma Z_0}{n^2} \tag{59}$$
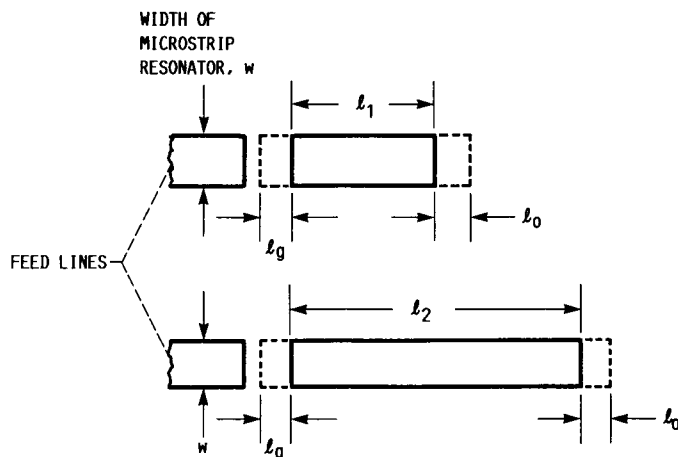
WIDTH OF
MICROSTRIP
RESONATOR, W

Figure 12.—Microstrip resonator pair and associated end effects.

with a corresponding reflection coefficient of

$$\Gamma_{r0} = \frac{(Z_i - \sigma Z_0) - n^2 Z_0}{(Z_i - \sigma Z_0) + n^2 Z_0} \tag{60}$$

Since

$$Z_i = Z_0 \left(\frac{1 + \Gamma_i}{1 - \Gamma_i} \right) \tag{61}$$

the reflection coefficient becomes

$$\Gamma_{r0} = \frac{(1 + \Gamma_i)/(1 - \Gamma_i) - \sigma - n^2}{(1 + \Gamma_i)/(1 - \Gamma_i) - \sigma + n^2} \tag{62}$$

Finally,

$$\Gamma_{r0} = \frac{K - \sigma - n^2}{K - \sigma + n^2} \tag{63}$$

where

$K = \kappa$, overcoupled

$K = 1/\kappa$, undercoupled

$K = 1$, critically coupled

Values of K and σ are known from previous measurements. A procedure for evaluating n^2 is described in the section entitled "Approximate Evaluation of Circuit Elements." Because of the fact that the measurement, or reference, plane is translated to the resonator terminals, the influence of the gap can be extracted.

Perturbation of Natural Resonant Frequency Due to Loading

As previously mentioned, the measured resonant frequency is shifted from the actual resonant frequency of the isolated circuit because of the reactance associated with the coupling mechanism. This "detuning" effect has little effect on the evaluation of Q but can appreciably distort the results of the permittivity calculations. The effect is most pronounced in the case of an overcoupled resonator for which κ is large. A good estimate of the unperturbed resonant frequency can be obtained by considering the coupled reactance in the calculation of ω_0. The total susceptance of the loaded resonator is

$$\chi_e = j \left(\omega C - \frac{1}{\omega L} - n^2 B \right) \tag{64}$$

where B is the gap susceptance.

At resonance, χ_e vanishes. This implies

$$\omega_{0a}^2 = \omega_{0n}^2 (1 + \omega_{0a} L n^2 B) \tag{65}$$

where ω_{0a} and ω_{0n} refer to the apparent and natural resonant frequencies, respectively. By continuing with the derivation and using the high Q approximation,

$$\frac{\omega_{0a}^2 - \omega_{0n}^2}{\omega_{0n}^2} = L n^2 B \omega_{0a} \approx 2\delta \tag{66}$$

$$\omega_{0a} - \omega_{0n} \approx \frac{\omega_{0n}^2 L n^2 B}{2} \tag{67}$$

$$\omega_{0a} \approx \omega_{0n} \left(1 + \frac{n^2 B}{2 C_0 \omega_{0n}} \right) = \omega_{0n} \left(1 + \frac{n^2 R_0 B}{2 Q_0} \right) \tag{68}$$

Finally, in terms of measurable quantities,

$$\omega_{0a} = \omega_{0n} \left(1 + \frac{\kappa X}{2 Q_0 Z_0} \right) \tag{69}$$

Thus, for an inductively coupled cavity, the natural resonant frequency is smaller than the apparent resonant frequency. Conversely, for a capacitively coupled cavity, the coupled susceptance is positive and the natural resonant frequency is larger. This result corresponds to the expression derived graphically by Kajfez (ref. 13) when using the approximation $(1 + \Delta)^{-1} \approx (1 - \Delta)$, and it is valid for high-Q cavities with reasonable coupling.

Comments on Frequency-Dependent Input Impedance

The circuit elements representing the microstrip resonator were assumed to be constant over the frequency range of interest. This condition resulted in the symmetric reflection coefficient response curves of figures 8 and 9. In practice, the observed response departs from the ideal situations because the lumped elements are, in fact, frequency dependent. From transmission line theory, the impedance of an open-circuit line near, but below, resonance looks inductive. Correspondingly, the line appears as a capacity just above resonance. This behavior is further complicated by the presence of small but finite loss. Consequently, the model previously developed is strictly accurate only at a single frequency, although it is a good approximation near resonance. A more accurate representation for describing the observed phenomenon can be obtained by replacing constant G_0 with a linearly frequency-dependent conductance G_e (ref. 14). As before, this element accounts for radiation resistance and material losses of the resonator. If the following variation is assumed,

$$G_e = G_0 (1 + \xi\delta) \tag{70}$$

where ξ is a small positive constant, and if the admittance increment at a small frequency excursion from resonance is considered,

$$\Delta Y_r = j \left(\delta\omega_0 C_0 + \frac{\delta\omega_0}{\omega_0^2 L_0} \right) \tag{71}$$

Then the new isolated resonator admittance becomes

$$Y_r = G_0(1 + \xi\delta) + j \left(\delta\omega_0 C_0 + \frac{\delta\omega_0}{\omega_0^2 L_0} \right) \tag{72}$$

When equations (3) and (9) are used, the admittance can be expressed as

$$Y_r = G_0[1 + \delta(\xi + j2Q_0)] \tag{73}$$

Finally, the input impedance at the gap terminals becomes

$$Z_i = \frac{\kappa Z_0}{1 + \delta(\xi + j2Q_0)} \tag{74}$$

The effect of the distortion is apparent in the reflection coefficient response curve. It is observed that the trailing edge falls back to unity more slowly. Additionally, the reflection coefficient minimum occurs slightly below the resonant frequency. By setting

$$\frac{d}{d\delta} |Y_i|^2 = 0 \tag{75}$$

the minimum impedance frequency can be found from

$$\delta = \frac{-\xi}{\xi^2 + 4Q_0^2} \tag{76}$$

These effects will, in general, have negligible consequences as far as the effect on Q and ϵ_{eff} is concerned. It is necessary, however, to be aware of the source of these effects when interpreting the measurements.

Experimental Results and Modeling

Approximate Evaluation of Circuit Elements

It is frequently desirable to solve for the various parameters representing the resonant system. Knowledge of the elements in the equivalent circuit is particularly useful for modeling

purposes. Empirical models for microstrip behavior, especially at discontinuities, are scarce at millimeter wavelengths.

Approximate values can be derived for each of the components included in the equivalent circuit. Following established reasoning, the quantitative description of the elements is valid near the resonant frequency.

It is essential to determine the transformer turns ratio in addition to evaluating the distributed resonator elements. A general impedance description of an open-circuit line is given by

$$Z_r = Z_0 \coth (\alpha + j\beta)\ell \tag{77}$$

which is the input impedance of the isolated microstrip resonator. By invoking the low-loss assumption once again and applying a useful trigonometric identity, the impedance becomes

$$Z_r \approx Z_0 \left(\frac{1 - j/\alpha\ell \cot \beta\ell}{1/\alpha\ell - j \cot \beta\ell} \right) \tag{78}$$

At the fundamental resonance, $\beta\ell \approx \pi$ and, since $\alpha\ell$ is small, the impedance is further simplified to

$$Z_r \approx Z_0 \left(\frac{-j \cot \beta\ell}{1 - j\alpha\ell \cot \beta\ell} \right) \tag{79}$$

Alternatively, in terms of admittance

$$Y_r \approx Y_0 \left(\frac{1 - j\alpha\ell \cot \beta\ell}{-j \cot \beta\ell} \right) \tag{80}$$

$$Y_r \approx Y_0(\alpha\ell + j \tan \beta\ell) \tag{81}$$

This is recognized as being comparable to equation (12). Hence, the reciprocal of the conductance G_0 becomes

$$R_0 \approx \frac{Z_0}{\alpha\ell} \tag{82}$$

By recalling that $\kappa = n^2 R_0/Z_0$ and using the relationship expressed by equation (51) with $\alpha_r = 0$, one obtains

$$n^2 \approx \kappa\alpha\ell \approx \frac{\kappa\beta\ell}{2Q_0} \approx \frac{\kappa\pi}{2Q_0} \tag{83}$$

Through the use of a similar approximation,

$$R_0 \approx \frac{2Z_0 Q_0}{\pi} \tag{84}$$

and it follows that the resonator capacitance and inductance must be

$$C_0 \approx \frac{\pi}{2Z_0\omega_0}; \qquad L_0 \approx \frac{2Z_0}{\pi\omega_0} \qquad (85)$$

The series loss σ is obtained from the detuned resonator reflection coefficient as described by equation (45). It is somewhat more difficult to evaluate the coupling reactance caused by complications from the feed line. A procedure to approximate jX_L is summarized in the section "Interpretation of Impedance Locus."

Results and Discussion of GaAs Microstrip Propagation Characteristics

By following the procedures outlined earlier, a number of resonator pairs were successfully characterized. Figures 13 and 14 depict the measured response for five sets of resonators
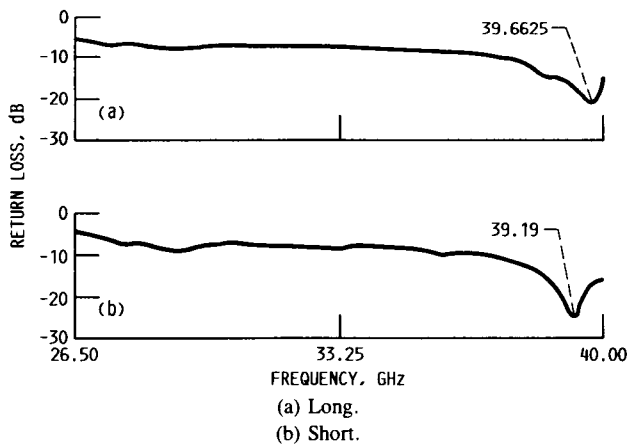

(a) Long.
(b) Short.

Figure 13.—S_{11} response of 5-mil-thick GaAs resonator from wafer 05pg001a.
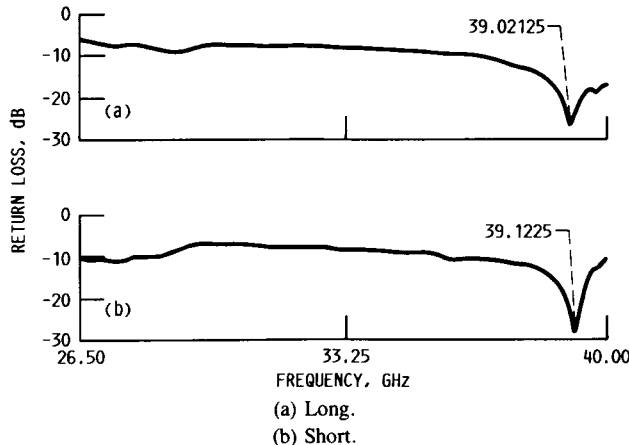

(a) Long.
(b) Short.

Figure 14.—S_{11} response of 10-mil-thick GaAs resonator from wafer 101f003a.

on both 5- and 10-mil-thick substrates. In each case, the resonance occurred near 40 GHz. The calculated permittivity revealed a significant discrepancy when compared with the theoretical value, causing a shift from the design frequency to the upper edge of the band. Consequently, the entire response could not be captured by the measurement system for the majority of tested cavities. This anomaly prevented a determination of Q for the 5-mil resonators; however, estimates for the 10-mil devices were possible.

Additional complications developed from the effects of the feed line and transition. Although the feed section will not alter f_0, an electrically long line significantly distorts the impedance locus and inhibits an accurate analysis. It is observed that the magnitude of S_{11} becomes irregular as a function of frequency because of periodic maxima and minima in return loss. In fact, if the line were infinitely long, the trace would become a cluster of points at the center of the Smith chart and appear matched. This phenomenon should be obvious from transmission-line theory because there are no reflections from an infinite line. The effect of the feed line was modeled with a hypothetical resonator equivalent circuit. A summary of the behavior is illustrated in figure 11.

The validity of the circuit element approximations of the section "Approximate Evaluation of Circuit Elements" was demonstrated by calculating the element values from a measured resonator. Results are presented in figure 15.
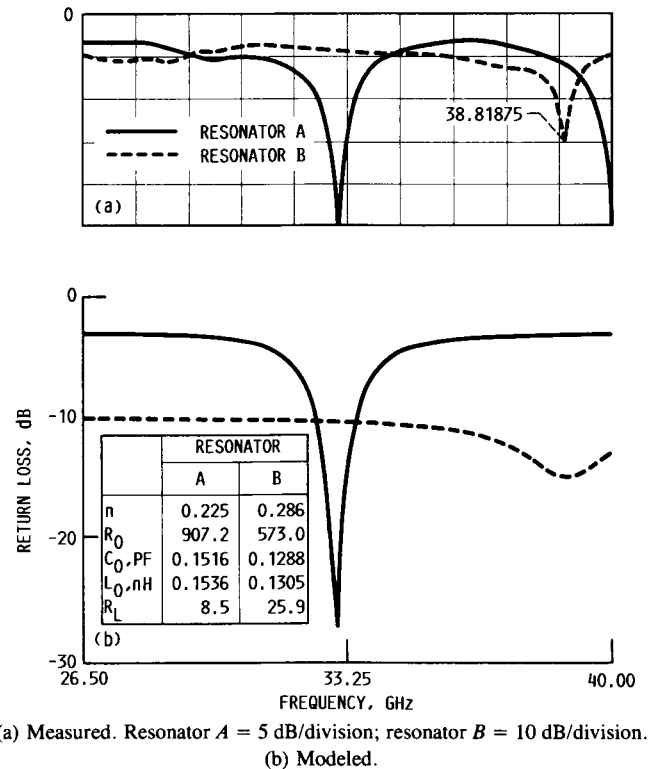
(a) Measured. Resonator A = 5 dB/division; resonator B = 10 dB/division.
(b) Modeled.

Figure 15.—Return loss characteristics for two 10-mil-thick GaAs resonators. Resonator A was scribed incorrectly causing an f_o of 32.98 GHz.

16

Modeled data correspond closely to the actual data despite the frequency-independent limitations of the lumped circuit, particularly when small losses are present. Quality factor Q data for the 10-mil GaAs are provided in figure 16. Owing to the small loss tangent, the dielectric Q curve did not appear on the graph, although its contribution is included in the results. The dominant effect of radiation is apparent and there is acceptable agreement with the theoretical solution. It should be noted that the calculated Q values of 18 and 24 are only approximate because the lack of symmetry in the response curve made determination of the 3-dB bandwidth difficult.

Unexpected results were obtained for the effective permittivity. As discussed earlier, the calculated values were substantially lower than the theoretical predictions. In fact, the measured permittivity at 40 GHz did not exceed the theoretical static effective permittivity. There are several possible explanations for the discrepancies. Because the actual Q values were relatively low (indicating moderate loss) there may have been a shift in the resonant frequency. More specifically, the exact solution of the resonant circuit would yield an expression for ω_0 dependent on Q such that

$$\omega_0' = \omega_0 \left[1 - \left(\frac{1}{2Q_0} \right)^2 \right]^{1/2} \tag{86}$$

Hence, for the resonators measured here, a shift in f_0 of approximately 12 MHz should be expected. In addition, the validity of the assumption regarding the independence of end effect on line length should be investigated further. Finally, some portion of the anomalous results could be attributed to anisotrophy of the substrate, although this is thought to be inconsequential. Table II summarizes the results for both 5- and 10-mil-thick GaAs resonators.

A useful empirical formula evolved from this work and from previous results (refs. 4 and 5). On the basis of the degree
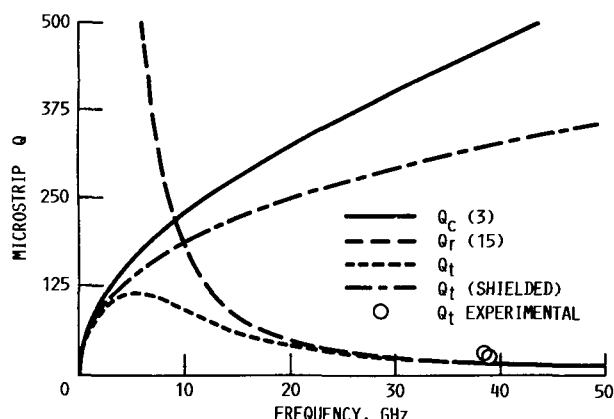

Figure 16.—Cumulative effects of various contributions to microstrip loss. The data are for half-wavelength resonators on 10-mil-thick GaAs with evaporated gold metalization.

TABLE II.—PERMITTIVITY DATA

Frequency, GHz	Substrate thickness, t, mil	
	5	10
	Effective permittivity, $\epsilon_{eff}(f)$	
39.072	-----	6.850
39.106	-----	6.920
39.241	-----	6.703
39.359	6.050	-----
39.426	6.288	-----

of coupling observed for the GaAs cavities and earlier polymeric substrate cavities, and taking into account other work by Edwards, the following expression should provide a gap dimension yielding loose-to-moderate coupling:

$$g = \frac{50 \log Z_0 \sqrt{h}}{Z_0 \sqrt{\epsilon_r - 1}} \text{ mil} \tag{87}$$

Conclusions

A thorough analytical procedure has been developed for evaluating the dynamic propagation characteristics of millimeter-wave microstrip lines. In order to complement the analytical procedure, an experimental method was devised that enabled the evaluation of the complex propagation constant. Data near 40 GHz for 5- and 10-mil thick GaAs microstrip resonators were obtained. As was evident from the measurements, accuracy of the method could be enhanced appreciably by using a de-embedding algorithm to relocate the reference (measurement) plane to the gap terminals. Furthermore, the importance of eliminating the effects of radiation is obvious from the results. The resonators should be enclosed in a waveguide below cutoff, or the experimental method outlined earlier should be used to minimize these effects. Simple but useful formulas provided for modeling the resonator behavior were shown to be acceptable. The approximations break down as coupling losses become excessive and Q values diminish. Significant fabrication obstacles limited the yield of testable devices; however, a workable process was developed for GaAs. In particular, advances were made in the areas of wafer thinning and electroplating.

The basic soundness of the methods was demonstrated and plans are under way for performing additional analysis through the use of a modified calibration technique. As the yield of the devices improves and suitable metrology techniques emerge, a statistically significant database will be developed. The long-range goal of this project is to provide appropriate high-frequency models for passive GaAs devices. These models are intended to support a growing need for CAD software related to millimeter-wave MMIC's.

Acknowledgments

References

1. Ginzton, E.L.: Microwave Measurements, McGraw-Hill, 1957.
2. Aitken, J.E.: Swept-Frequency Microwave Q-Factor Measurement. IEEE Proc., vol. 123, no. 9, Sept. 1976, pp. 855–862.
3. Pucel, R.A.; Masse, D.J.; and Hartwig, C.P.: Losses in Microstrip. IEEE Trans. Microwave Theory Tech., vol. MTT–16, no. 6, June 1968, pp. 342–350. "Correction to 'Losses in Microstrip'," ibid., no. 12, Dec. 1968, p. 1064.
4. Edwards, T.C.: Foundations for Microstrip Circuit Design. John Wiley and Sons, 1981.
5. Romanofsky, R.R., et al.: An Experimental Investigation of Microstrip Properties on Soft Substrates from 2 to 40 GHz. 1985 IEEE MTT–S International Microwave-Symposium Digest, IEEE, 1985, pp. 675–678.
6. Romanofsky, R.R.; and Shalkhauser, K.A.: Universal Test Fixture for Monolithic Millimeter-Wave Integrated Circuits Calibrated With an Augmented TRD Algorithm. NASA TP–2875, 1989.
7. Montgomery, C.G.; Dicke, R.H.; and Purcell, E.M.: Principles of Microwave Circuits, McGraw-Hill, 1948.
8. Kajfez, D.; and Hwan, E.J.: Q-Factor Measurement With Network Analyzer. IEEE Trans. Microwave Theory Tech., vol. MTT–32, no. 7, July 1984, pp. 666–670.
9. Sucher, M.; and Fox, J.: Handbook of Microwave Measurements, Vol. II, Polytechnic Press, New York, 1963.
10. Gupta, C.; Easter, B.; and Gopinath, A.: Some Results on the End Effects of Microstriplines. IEEE Trans. Microwave Theory Tech., vol. MTT–26, no. 9, Sept. 1978, pp. 649–652.
11. James, D.S.; and Tse, S.H.: Microstrip End Effects. Electron. Lett., vol. 8, no. 2, Jan. 27, 1972, pp. 46–47.
12. Toncich, S.; and Collin, R.E.: Data Reduction Method for Q Measurements of Strip-Line Resonators. (WGR–86–5, Case Western Reserve University, NASA Grant NCC3–2a) NASA CR–176895, 1986.
13. Kajfez, D.: Correction for Measured Resonant Frequency of Unloaded Cavity. Electron. Lett., vol. 20, no. 2, Jan. 19, 1984, pp. 81–82.
14. Jordain, E.; and Balmain, K.: Electromagnetic Waves and Radiating Systems. 2nd ed., Prentice-Hall, Inc., 1968.
15. Denlinger, E.J.: Losses of Microstrip Lines. IEEE Trans. Microwave Theory Tech., vol. MTT–28, no. 6, June 1980, pp. 513–522.

NASA
National Aeronautics and
Space Administration

Report Documentation Page

1. Report No. NASA TP-2899	2. Government Accession No.	3. Recipient's Catalog No.

4. Title and Subtitle	5. Report Date
Analytical and Experimental Procedures for Determining Propagation Characteristics of Millimeter-Wave Gallium Arsenide Microstrip Lines	March 1989
	6. Performing Organization Code

7. Author(s)	8. Performing Organization Report No.
Robert R. Romanofsky	E-4273
	10. Work Unit No. 506-44-2C

9. Performing Organization Name and Address	11. Contract or Grant No.
National Aeronautics and Space Administration Lewis Research Center Cleveland, Ohio 44135-3191	
	13. Type of Report and Period Covered

12. Sponsoring Agency Name and Address	Technical Paper
National Aeronautics and Space Administration Washington, D.C. 20546-0001	14. Sponsoring Agency Code

15. Supplementary Notes

16. Abstract

In this report, a thorough analytical procedure is developed for evaluating the frequency-dependent loss characteristics and effective permittivity of microstrip lines. The technique is based on the measured reflection coefficient of microstrip resonator pairs. Experimental data, including quality factor Q, effective relative permittivity, and fringing for 50-Ω lines on gallium arsenide (GaAs) from 26.5 to 40.0 GHz are presented. The effects of an imperfect open circuit, coupling losses, and loading of the resonant frequency are considered. A cosine-tapered ridge-guide test fixture is described. It was found to be well suited to the device characterization.

17. Key Words (Suggested by Author(s))	18. Distribution Statement
Microstrip attenuation Dispersion Microstrip Q Ridge-guide transition	Unclassified – Unlimited Subject Category 33

19. Security Classif. (of this report) Unclassified	20. Security Classif. (of this page) Unclassified	21. No of pages 24	22. Price* A03